Journal of Catalysis 356 (2017) 65–74

Contents lists available at ScienceDirect

Journal of Catalysis

journal homepage: www.elsevier.com/locate/jcat

Preparation and particle size effects of Ag/α-Al_2O_3 catalysts for ethylene epoxidation

J.E. van den Reijen [a], S. Kanungo [b], T.A.J. Welling [c], M. Versluijs-Helder [a], T.A. Nijhuis [b,1], K.P. de Jong [a], P.E. de Jongh [a,*]

[a] Inorganic Chemistry and Catalysis, Debye Institute for Nanomaterials Science, Utrecht University, Utrecht, The Netherlands
[b] Laboratory of Chemical Reactor Engineering, Department of Chemical Engineering and Chemistry, Eindhoven University of Technology, Eindhoven, The Netherlands
[c] Soft Condensed Matter, Debye Institute for Nanomaterials Science, Utrecht University, Utrecht, The Netherlands

ARTICLE INFO

Article history:
Received 26 July 2017
Revised 30 September 2017
Accepted 3 October 2017
Available online 6 November 2017

Keywords:
Ethylene epoxidation
Silver
α-Alumina
Catalyst design
Ethylene oxide
Particle size effect

ABSTRACT

Currently, for the industrial ethylene epoxidation α-alumina supported silver catalysts are the only catalyst of choice. We demonstrate a novel method to produce these catalysts with different silver particle sizes, but without changing other key parameters that may affect the catalytic performance such as support specific surface area or metal precursor. α-Alumina was impregnated with a silver oxalate solution, and was subsequently dried and treated in different gas atmospheres and at different temperatures to tune the silver particle sizes in the range of 20–500 nm. Particles of 20 nm exhibited a lower turnover frequency than particles of 70 nm and larger, which exhibit a constant turnover frequency, in accordance with results in literature. However, the selectivity, when measured at constant conversion, was particle size independent. This is the first time that the effect of the particle size on the selectivity of ethylene epoxidation is reported at constant conversion. This was made possible by a new method of producing supported silver catalysts, which we expect that is also applicable for silver catalysts with other supports and for the preparation of other supported metal catalysts.

1. Introduction

Ethylene epoxidation using silver catalysts is an important industrial process with an annual worldwide production of ethylene oxide of 25 · 10^6 ton in 2013 [1,2] Ethylene oxide (EO) is used as a disinfectant and sterilizing agent, but the most important consumption of EO is for hydration to ethylene glycol, which is the main component in antifreeze and a precursor for polyesters and polyurethanes [3]. The silver catalysts used for EO production in industry consist of promoted α-alumina supported silver particles with a size range of 100–1000 nm [1,4]. The role of the support in the catalyst is to enable the preparation of small metal particles and to prevent deactivation by sintering [5]. α-Alumina is the most stable crystal phase of alumina. It exhibits a low density of surface groups, typically <1 OH nm^{-2}, and a specific surface area below 10 m^2 g^{-1} [6]. Both characteristics limit the total amount of surface OH groups [7–9]. Lee et al. and Mao et al. established that side-reactions partially occur on surface OH groups of the support; hence, the use of α-alumina as a support limits these unwanted reactions [10,11].

Industrial catalysts typically consist of supported silver catalysts with 100–1000 nm particle sizes. Furthermore a moderator (chlorine containing compound) is used in the process and promotors (Cs, Re, S, etcetera) are added to the catalyst. Industrial catalysts nowadays give high selectivities toward ethylene oxide; sometimes exceeding 90% [12,13]. These selectivities exceed the previously assumed theoretical maximum of $^6/_7$ or 85.7% associated with the model that Kilty and Sachtler proposed in the 1970s. In their model molecularly adsorbed oxygen is responsible for the selective oxidation reaction, leading to the formation of an epoxide and an atomically adsorbed oxygen. Six of these adsorbed oxygen atoms would be involved in the unselective oxidation of ethylene, leading to carbon dioxide and water [14,15]. Therefore, for every six ethylene oxide molecules produced, one ethylene molecule would be fully oxidized. While this mechanism was supported for some years by some groups [16,17], selectivities higher than expected based on this model were achieved with promoted catalysts shortly after this model was proposed [14,18,19]. Therefore, another mechanism based

* Corresponding author.
E-mail address: P.E.deJongh@uu.nl (P.E. de Jongh).
[1] Present address: SABIC, STC Geleen, PO Box 5151, 6130 PD Sittard, The Netherlands.

https://doi.org/10.1016/j.jcat.2017.10.001
0021-9517/

on atomic oxygen to describe the ethylene epoxidation reaction was required [18,20].

Computational results supported an oxometallocycle (OMC) mechanism, in which a key step is the formation of an OMC surface intermediate: an ethylene molecule adsorbed on an ensemble of surface oxygen atoms and a metal site [21,22]. This OMC can then form ethylene oxide (EO) or acetaldehyde, of which the latter is subsequently fully oxidized over silver [11]. However, while EO selectivities around 50% observed with model catalysts fit the competitive formation of acetaldehyde and EO, the observed increase in selectivity with increasing oxygen coverage cannot be explained by the OMC mechanism [13,23].

Özbek et al. propose the need for an oxidized silver surface. An Eley–Rideal (E-R) mechanism over an Ag_2O(0 0 1) crystal surface would open up a fully selective reaction pathway to ethylene oxide. In this mechanism no acetaldehyde formation occurs when no oxygen vacancies are present. However, in the presence of these oxygen vacancies, an OMC mechanism is followed, favoring acetaldehyde formation [13,23]. Under real reaction conditions the competitive adsorption of oxygen and ethylene on these oxygen vacancies is therefore key. The E-R mechanism therefore is in agreement with high selectivities toward ethylene oxide observed, while also predicting the dependence of selectivity on the oxygen coverage [24].

The OMC and the direct E-R mechanisms do not take the support into account, but propose that EO isomerization occurs on the silver surface [13,23]. However, the support is believed to catalyze the ring opening of EO, providing an additional pathway reducing the overall selectivity [25]. In all cases, the silver surface is believed to promptly oxidize acetaldehyde to form carbon dioxide and water.

Various experimental studies, such as Verykios et al., showed a particle size dependent activity in the oxidation of ethylene over silver catalysts [25]. This trend was suggested to be caused by inherently different activities of different silver crystal planes [17,24,26]. While initially supporting this claim [17], Campbell reported similar epoxidation rates on both crystal planes in 1985 [27].

Also the influence of particle size and crystal facets on selectivity is debated. Recently Christopher et al. argued, based on studies on spheres containing both Ag(1 0 0) and Ag(1 1 1) facets, and cubes and rods containing primarily Ag(1 0 0) facets, that Ag(1 0 0) surfaces preferentially lead to EO and Ag(1 1 1) surfaces lead to the formation of acetaldehyde [24,28]. However, a complication is that particle size effects on activity and selectivity are often obscured by measuring at different conversions. Conversion levels (which depend on activity) have a large influence on the selectivity (as we will demonstrate later in this paper) and hence a careful deconvolution of the two different factors parameters is necessary.

Particle size effects are common in catalysis, but the metal particle size of the active metal below which the specific activity decreases is generally smaller than 10 nm. A well-known example of reported particle size effects are gold catalysts in the epoxidation of propylene. In this reaction small particles (<2 nm) are highly active, but unselective, while large particles (>4 nm) are hardly active, leading to an optimal particle size of 2–4 nm. Similarly cobalt catalyzed Fischer-Tropsch synthesis and copper catalyzed methanol synthesis exhibit optimal particle sizes [29,30]. In these reactions, metal particles smaller than 6–8 nm exhibit significantly lower turnover frequencies (TOF) than larger particles, while larger metal particles exhibit particle size independent TOF's [29]. The CO activation requires an ensemble of surface atoms, which are unique to step-edge sites (B5-type sites), which in turn are rare on particles smaller than 10 nm [31,32]. In ethylene epoxidation the particle size effect follows a trend similar to the Fischer-Tropsch reaction, but it occurs at particle sizes an order of magnitude larger.

Already in 1975 Wu and Harriot reported a decreasing surface-specific rate of both epoxidation and combustion with increasing particle size in the range of 3–50 nm [28]. In 1980, Verykios et al. observed a minimal specific rate of oxidation (mol m^{-2} s^{-1}) at a particle size of 50–70 nm. Both groups reported an increasing selectivity with particle size over the entire size range [33]. At the time, these results were controversial and their conclusions were disputed by Sajkowski and Boudart who claimed that the observed differences in specific reactions rates were too small to be significant and results to be influenced by contaminations. They expected the presence of contaminations to act as a poison due to unexpectedly low turnover rates reported by Verykios et al. [34].

Verykios et al. synthesized catalysts with small silver particles supported on materials with different specific surface area. They heat treated these catalysts at different temperatures for different calcination times to obtain sets of catalysts with different particle sizes. In a later paper from the same group, they synthesized catalysts with different weight loadings on a single support batch to obtain silver particles with different particle sizes. Using this method, they prevented contaminations that may be introduced by using different support materials and segregation of contaminations during the heat treatment [25,35]. In this second study, they obtained a maximum specific rate of epoxidation and combustion at silver particle sizes of about 40–50 nm, contradicting their earlier results [35].

In this second paper, the selectivity to ethylene oxide increased slightly with particle size, which they attributed to differences in the rates of the secondary reactions for different particle sizes. Since the activity showed a particle size dependence, the partial pressure of ethylene oxide differs per sample. When corrected for these secondary reactions with a rate of EO oxidation obtained from experiments over bare supports, they obtained a slight decrease in selectivity with particle size [32]. They believed that the actual particle size dependency of the selectivity toward ethylene oxide lies somewhere between the observed and the corrected trend [35].

Since the late 90s, the particle size dependency of the activity has been largely accepted to exhibit a maximum activity per gram of silver at particle sizes of 50–70 nm for supported silver catalysts [35–37]. However, the cause of this effect was still under discussion. In 1997 the group of Bal'zhinimaev attributed the typical particle size dependence to different electronic states of the silver surfaces. With XPS they showed the formation of an anionic oxygen species on larger particles, while these species were not present on silver particles smaller than 50 nm [38,39]. These results showed a clear correlation with ^{109}Ag-NMR results and catalytic data for the epoxidation reaction over these catalysts [40] and correlates well with the observation of Akella and Lee in 1984 that correlates oxygen coverage with selectivity [41].

On silver surfaces nucleophilic oxygen is believed to coexist with electrophilic oxygen species, and both are required for an active and selective epoxidation catalyst [20,37,39,42]. The former is required for ethylene adsorption, while the latter activates the ethylene double bond and is inserted to form EO [43,37]. These species were identified as subsurface oxygen and adsorbed oxygen species on silver oxide surfaces [18,44]. This observation fits the alternative reaction pathway proposed by Grant and Lambert in 1985 [20]. In 2011 Özbek et al. proposed that in the absence of oxygen vacancies the reaction occurs via a selective, direct reaction (Eley–Rideal) pathway, while the reaction occurs via an OMC pathway when oxygen vacancies are present. This reaction explains the competitive formation of acetaldehyde and EO based on the oxygen species present [23].

Not many studies address the effects of particle size on selectivity and most available literature report an increase in selectivity with particle size [25,36,37]. However, in the academic literature the selectivity is generally reported at a constant temperature and hence at widely varying conversions. To our knowledge, only the paper of Lee et al. tried to correct for the inevitable artifacts introduced by this way of reporting [10]. Their method to correct for the secondary reactions, by subtracting an ethylene oxide oxidation rate obtained over bare supports, illustrates clearly how difficult it is to extract the intrinsic particle size dependency of the catalytic performance for this type of catalysts.

As was shown by the work of Verykios et al. discussed earlier, intrinsic particle size effects are often obscured by the fact that other parameters change as well [4,10,25,35]. Reported methods for obtaining different particle sizes involve changing the metal precursor, the support material and/or the weight loading [10,25,35,45,46].

Therefore, studying the performance of a set of catalysts having different particle sizes, but obtained from the same precursor on the same support and maintaining a constant metal loading, is highly desired. In the present paper we describe a synthesis method for α-alumina supported silver catalysts with different particle sizes. Building on previous knowledge [47–49], we use different gas atmospheres and temperatures during heat treatment of the catalyst precursor to tune the particle size, while the support type, support surface area and metal loading are kept constant. Precursor decomposition in hydrogen atmosphere yielded significantly smaller particles than heating in air or nitrogen atmosphere. Different gas atmospheres combined with heat treatments at different temperatures and times, yielded a range of different particle sizes. The obtained catalysts were tested in the ethylene epoxidation reaction to investigate the intrinsic effects of the particle size on activity and selectivity.

2. Methods

2.1. Silver precursor

Silver oxalate was used as the silver precursor for the impregnation of the alumina support. To synthesize the silver oxalate, 2.00 g silver nitrate (≥99.0%, Sigma Aldrich) was dissolved in 20 mL milliQ water and added to oxalic acid solution at 60 °C. The latter solution was obtained by dissolving 1.48 g oxalic acid dihydrate (99%, Sigma Aldrich) (2:1 M ratio) in 40 mL milliQ water at 60 °C [50–52]. Silver oxalate started to precipitate immediately, and was obtained after centrifugation and three times washing with milliQ water and once with ethanol. The white powder was dried overnight at 60 °C under static air.

2.2. Catalyst preparation

Extrudates of α-alumina (surface area 8 m^2 g^{-1}; pore volume 0.4 mL g^{-1}, AL4196E, BASF) were crushed to roughly 400 μm grain size with a size distribution as listed in Table S1. 5.0 g of α-alumina support grains was dried overnight at 120 °C in static air before impregnation. The dry powder was impregnated with 1.24 g dry silver oxalate dissolved in 2.0 mL of 0.73 g/g milliQ ethylene diamine(*en*)/water (1:4:16 mol ratio $Ag_2C_2O_4$: *en:* H_2O) mixture and subsequently dried in static air at 60 °C [12,53,54]. To favor a homogeneous distribution of silver over the support, the powder was mixed during drying [55]. After drying for 5, 10 and 30 min the powder was mixed manually before leaving the powder overnight to dry.

The impregnated alumina ($[Ag(en)_2]_2C_2O_4/\alpha\text{-}Al_2O_3$) was heated using different conditions, typically 150 mg in a U-shaped flow reactor at atmospheric pressure. After thermal treatment the catalysts were again crushed, and sieved to a 38–90 μm sieve fraction. The resulting catalysts consisted of 15 wt% silver on α-alumina and are denominated as $AgAl_2O_3$_atm_flow. The gas atmosphere during the temperature treatment is represented in atm, given in volume percentages in nitrogen and the flow in mL min^{-1}. The heating rate, final temperature and dwell time during calcination are 5 °C min^{-1}, 215 in °C and 2 h except for the catalyst denoted as $AgAl_2O_3$_350_100%N2_0, which was heated to 350 °C with 1 °C min^{-1}, and kept at this temperature for 24 h. An overview of all catalysts discussed in this paper is listed in Table 1.

2.3. Characterization

The crystalline phases were analyzed with X-ray Diffraction (XRD) using a Bruker D8 Advance diffractometer equipped with a Co Kα source (λ = 0.1789 nm) in the angle range from 20° to 90° in 2θ and a characterization procedure in the DIFFRAC Eva software (Bruker AXS). This analysis primarily served to verify the formation of silver oxalate and silver metal respectively.

Elemental analysis was performed with induced coupled plasma-optical emission spectrometry (ICP-OES) and X-ray fluorescence (XRF), using a ThermoFischer Scientific ICP-OES and a Thermo ARL 9400 sequential XRF at Department of Earth Sciences (Utrecht University) respectively. The weight loss during heat treatment was measured using thermal gravimetric analysis (TGA) performed in a Perkin Elmer Pyris 1 TGA under a 10 mL min^{-1} flow of oxygen or hydrogen in 45 mL min^{-1} argon or a flow of 55 mL min^{-1} pure argon. For these experiments the temperature was increased from 50 °C to 250 °C with a heating ramp of 1 °C min^{-1}. The decomposition products were analyzed using a Pfeiffer Vacuum OmniStar mass spectrometer.

The size and spatial distribution of the obtained silver particles were measured using transmission electron microscopy (TEM) and scanning electron microscopy (SEM). The images were obtained using a FEI Tecnai-12 transmission electron microscope and a FEI XL30 SFEG scanning electron microscope respectively. The obtained images were processed using iTEM Soft Imaging System software [56]. UV/VIS spectra of the supported silver catalysts were obtained using a Varian CARY 500 Scan UV–Vis–NIR spectrophotometer with an integrating sphere detector. In a typical analysis, 30 mg of 15 wt% $Ag/\alpha\text{-}Al_2O_3$ catalyst was diluted with 600 mg

Table 1
Overview of the $Ag/\alpha\text{-}Al_2O_3$ catalyst samples were labeled as $AgAl_2O_3$_atm_flow.

Reducing atmosphere	Inert atmosphere	Oxidizing atmosphere
$AgAl_2O_3$_100%H2_0	$AgAl_2O_3$_100%N2_0	$AgAl_2O_3$_100%O2_0
$AgAl_2O_3$_100%H2_10	$AgAl_2O_3$_100%N2_10	$AgAl_2O_3$_100%O2_10
$AgAl_2O_3$_100%H2_25	$AgAl_2O_3$_100%N2_25	$AgAl_2O_3$_100%O2_25
$AgAl_2O_3$_100%H2_50	$AgAl_2O_3$_100%N2_50	$AgAl_2O_3$_100%O2_50
$AgAl_2O_3$_100%H2_100	$AgAl_2O_3$_100%N2_100	$AgAl_2O_3$_100%O2_100
$AgAl_2O_3$_50%H2_0	–	$AgAl_2O_3$_50%O2_0
$AgAl_2O_3$_50%H2_10	–	$AgAl_2O_3$_50%O2_10
$AgAl_2O_3$_50%H2_50	–	$AgAl_2O_3$_50%O2_50
$AgAl_2O_3$_50%H2_100	–	$AgAl_2O_3$_50%O2_100
$AgAl_2O_3$_20%H2_50	–	$AgAl_2O_3$_20%O2_50
$AgAl_2O_3$_8.5%H2_0	–	$AgAl_2O_3$_8.5%O2_0
$AgAl_2O_3$_8.5%H2_10	–	$AgAl_2O_3$_8.5%O2_10
$AgAl_2O_3$_8.5%H2_25	–	$AgAl_2O_3$_8.5%O2_25
$AgAl_2O_3$_8.5%H2_50	–	$AgAl_2O_3$_8.5%O2_50
$AgAl_2O_3$_8.5%H2_100	–	$AgAl_2O_3$_8.5%O2_100
–	$AgAl_2O_3$_350_100%N2_0*	–

* Heated with 1 °C min^{-1} to 350 °C, and kept at this temperature for 24 hours in static nitrogen.

pristine α-Al_2O_3 (1 m^2 g^{-1}, −100 mesh, Sigma Aldrich) and ground to a fine powder before taking a spectrum in the 200–750 nm range. A background measurement of pristine α-Al_2O_3 was performed and subtracted from the obtained spectra. A simplified model of the catalyst was simulated using FDTD Solutions 8.0 software package (Lumerical) to compute UV/Vis spectra. Simulations consisted of a single silver particle in an environment of 0, 10, 20, 25, 33.33, 50, 75 and 100% of α-alumina in air at 300 K. The silver particle size was varied between 10 and 140 nm with steps of 10 nm. A three-dimensional non-uniform mesh with a grid size of 0.5 nm was used for the silver particle and its direct surroundings. The localized surface plasmon resonance was calculated in the 200–800 nm range from a total field scattered field source. The simulation was run until converged below 1e−05. The data was fitted with a second order polynomial surface (R^2 = 0.9995). The model was in good agreement with the work from Mock et al. for spherical silver particles [57].

2.4. Catalytic testing

Catalytic tests were performed with metal particle sizes ranging from 20 to 500 nm obtained. As a reference a Cs-promoted commercial catalyst containing 18 wt% Ag on α-Al_2O_3 [58], was measured under the same reaction conditions. Typically 150 mg of a 38–90 μm sieve fraction of the material was loaded between two layers of quartz wool in a quartz reactor with a 4 mm internal diameter. The sample was heated to 180 °C in a flow of 15 mL min^{-1} of 8.5% oxygen and 30% ethylene in helium, corresponding to a gas hourly space velocity of 6000 mL g_{cat}^{-1} h^{-1}. After one hour the temperature was increased stepwise to 270 °C followed by 1 h at 190 and 180 °C respectively (1 h at 180 °C, 1 h at 190 °C, 1 h at 200 °C, 1 h at 215 °C, 1 h at 230, 2 h at 250 °C, 3 h at 260 °C, 3 h at 270 °C, 1 h at 190 °C and 1 h at 180 °C) [12]. The outlet gases of the reaction were analyzed every 30 min by an online Compact GC (Interscience) equipped with a Porabond Q column and a Molsieve 5A column in two separate channels, both with a thermal conductivity detector (TCD). Conversion data were calculated from data retrieved at 190 and 200 °C after steady state was reached, a more detailed description of the calculations can be found in the supplementary information. Selectivity data were obtained at an ethylene conversion of 2.8%.

3. Results and discussion

3.1. Particle size analysis

Typical images of Ag/α-Al_2O_3 catalysts, obtained using electron microscopy, are shown in Fig. 1. The micrographs show the samples treated in 50 mL min^{-1} flow of 100% H_2, 100% N_2 and 100% O_2 respectively. In the bright-field TEM micrograph of the hydrogen treated sample in the left frame, the alumina support can be seen in dark grey spots and has a particle size of several hundreds of nanometers. Silver particles are visible as smaller and darker spots, with sizes up to 100 nm. Examples are indicated with circles. In the SEM micrographs of samples obtained after treatment in nitrogen and oxygen displayed in the frames in the middle and on the right, the alumina support surface is visible as light grey rounded particles. The silver particles are bright white spots, isotropic in shape, and not strongly facetted. The silver particle size distributions, shown in the lower frames, are significantly different for different heat treatment conditions. Note the presence of particles larger than 150 nm in the sample treated in oxygen containing atmosphere. The particle size distributions in Fig. 1 are typical for this type of catalysts [59].

As it is challenging to obtain results on a statistically relevant amount of sample using electron microscopy, we explored UV/Vis spectroscopy as a bulk analysis technique for validation. In Fig. 2 the UV/Vis spectra of selected catalysts can be found, with

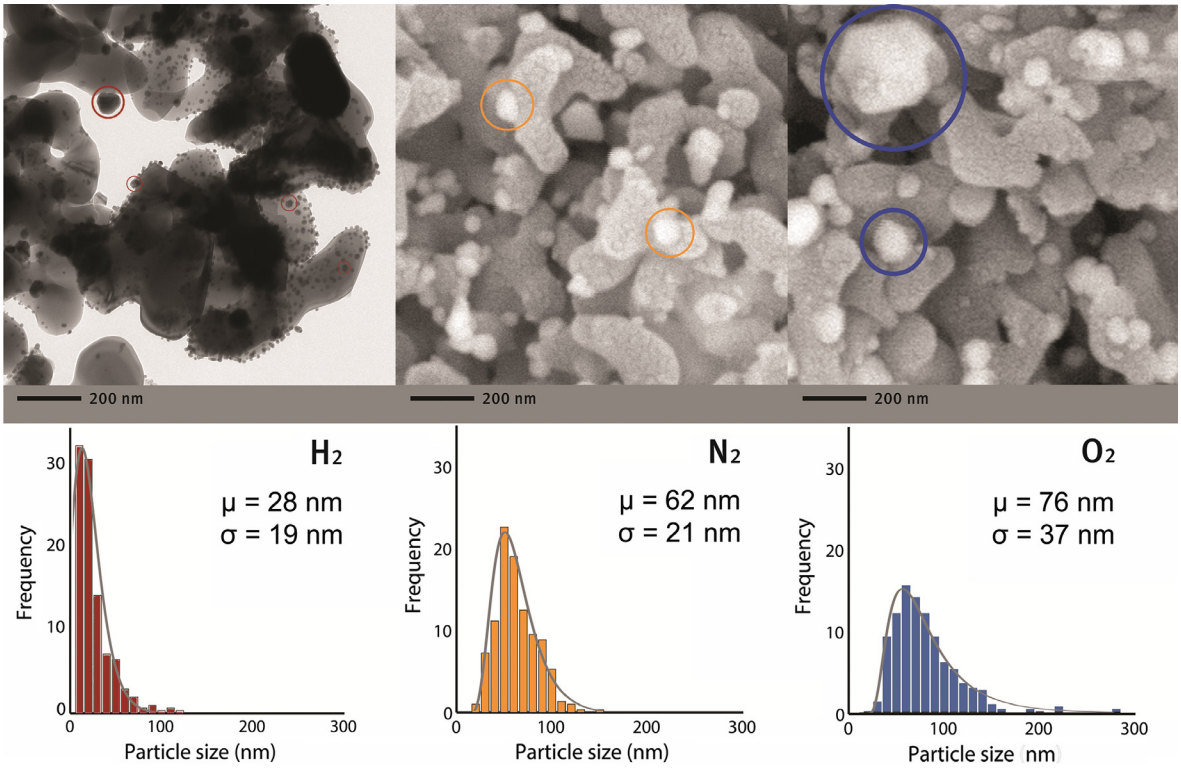

Fig. 1. TEM and SEM images of Ag/α-alumina with a range of particle sizes. From left to right: $AgAl_2O_3$_100%H2_50 (TEM), $AgAl_2O_3$_100%N2_50 (SEM) and $AgAl_2O_3$_100% O2_50 (SEM).

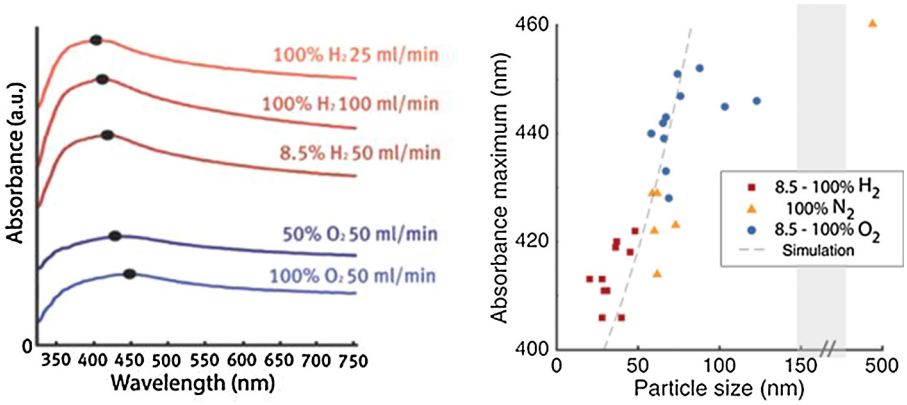

Fig. 2. (left) UV/Vis spectra of Ag/α-alumina with a range of particle sizes. Displayed spectra obtained from (from top to bottom) $AgAl_2O_3$_100%H2_25, $AgAl_2O_3$_100%H2_100, $AgAl_2O_3$_8.5%H2_50, $AgAl_2O_3$_50%O2_50, and $AgAl_2O_3$_100%O2_50. The spectra are offset for clarity. (right) Surface plasmon resonance peak position as determined by UV/Vis compared to the particle size of silver particles on α-alumina as determined by electron microscopy. Theoretical SPR peak position obtained from simulations of silver particles in a 60% air, 40% α-alumina environment obtained with Lumerical software package is indicated by dotted grey line. Catalyst $AgAl_2O_3$_1_350_100%N2_24h_0 with large silver particle size added as a reference.

the peak maxima of the SPR peak in the obtained UV/Vis spectra indicated with a black dot. The spectra exhibit a broad peak in the 300–750 nm range corresponding to the surface plasmon resonance (SPR) of the silver particles on the catalyst surface. The position of the peak depends on the silver particle size and shape and on the dielectric constant of the direct surroundings of the silver particles. When the particles are assumed to be spherical, a SPR peak with a maximum in the 380–500 nm range is expected, shifting to longer wavelengths for larger particles [57,60]. Average silver particle sizes above about 100 nm correspond to grey samples.

The peak maximum shifts to longer wavelengths when going from samples obtained from heat treatment in reducing gas atmospheres to samples obtained in oxidizing gas atmospheres. The intensity of the SPR peak decreases with increasing particle size and the peak position becomes more difficult to determine [47,48]. This is in accordance with computational predictions of the UV/Vis spectra of spherical silver particles of different sizes on a alumina support performed by us and with literature [61,62].

In the right frame of Fig. 2 the SPR peak position of differently heat treated samples is plotted against the surface averaged particle size obtained by electron microscopy. The dotted line is obtained from computational results of the SPR peak maximum for different silver particle sizes. The resulting peak maximum can only be used to predict an average silver particle size, as only a single silver particle is simulated for each size. The effects of particle and size distributions are therefore not taken into account. Catalysts with the smallest silver particle sizes, like the samples obtained by heat treatment in hydrogen, show intense and sharp SPR peaks in the UV/Vis spectra with maxima at relatively low wavelengths. Catalysts with a larger average particle size in SEM, like the samples treated in oxygen containing atmosphere show a much broader peak with a SPR peak maxima at higher wavelengths. UV/Vis spectra with SPR peaks up until circa 440 nm, or silver particle sizes of circa 75 nm, are intense enough for a proper estimation of the average silver particle size. For larger particle sizes the values obtained using electron microscopy start to deviate strongly from the value from UV/Vis due to the low absorption coefficient of these large silver particles. A reference catalyst with a surface averaged particle size of 500 nm was analyzed; this catalyst is denoted as $AgAl_2O_3$_350_100%N2_0. The reference catalysts exhibited a weak surface plasmon resonance at 460 nm. This confirmed that it is possible to estimate the silver particle size for catalysts with average silver particles up to 75 nm.

3.2. Effect of gas flow during precursor decomposition

An overview of the surface averaged particle size of samples treated under different gas atmospheres and gas flows are given in Fig. 3. Particle sizes obtained both from electron microscopy techniques as well as from UV/Vis are included. The average particle size clearly increases going from more reducing to more oxidizing atmospheres. When the heat treatment is performed in static conditions, the final silver particle size is slightly higher than for catalysts treated in a gas flow. A linear fit excluding the data from catalysts obtained under static conditions is added as dashed line as a guide for the eye.

The trends observed in Fig. 3 show a pronounced effect of gas atmosphere during heat treatment, while in general, the effect of flow is less prominent. The slightly higher average silver particle size in catalysts obtained in static conditions is attributed to the poor removal of decomposition products, while at intermediate or high flows this removal is facilitated. Overall, the method of heat treatment in different atmospheres is successful in producing catalysts with a broad range of silver particle sizes. A small amount of

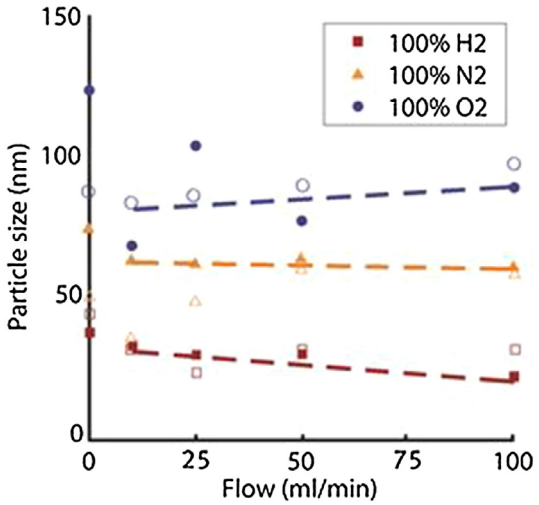

Fig. 3. Particle size of silver particles on α-alumina as determined by electron microscopy (closed symbols) and UV/Vis (open symbols) after heat treatment in different gas atmospheres (hydrogen or oxygen in nitrogen) with different flow rates over 150 mg of sample. Dashed lines added as a guide for the eye.

hydrogen, exemplified by 8.5% hydrogen in nitrogen, already results in very small particles, while the size of the silver particles increasing with increasing oxygen partial pressure, as can be seen in Fig. S2 in the supplementary information.

3.3. Decomposition of silver precursor

In Fig. 4 the weight loss during heating of the $[Ag(en)_2]_2C_2O_4/\alpha$-alumina catalyst precursor in different gas atmospheres is plotted. Prior to analysis the sample was dried to remove water and ethylene diamine. This resulted in the formation of $Ag_2C_2O_4/\alpha$-Al_2O_3 which should exhibit a weight loss of 5.8% when decomposed fully into Ag/α-Al_2O_3 and CO_2. The total weight loss observed in the thermographic analysis (TGA) is 4.8%, which agrees within the error of the measurement with the expected weight loss. In the derivative of the TGA (DTG) a sharp peak can be seen, which represents decomposition of the complex, with a small shoulder at higher temperatures. Between 150 and 200 °C an additional decomposition peak is visible in all three cases. The onset decomposition temperature is slightly higher for inert and oxidizing atmospheres (for the main decomposition peak at 73 °C for H_2 versus 84 and 86 °C for argon and air respectively). At 250 °C a sharp weight loss of 0.4% is observed in the measurement in oxidizing atmosphere, while no such decomposition step is visible in inert or reducing atmospheres. The final weight is referenced to the sample measured in inert atmosphere, as the samples after heat treatment all resulted in 15 wt% Ag/α-alumina.

The fact that the initial weight of some samples exceeds 100% at the start of the measurement is attributed to the residual water content of the sample and not fully complete removal of ethylene diamine prior to analysis. Mass spectrometry analysis (Fig. S3) predominately shows the formation of CO_2. Less than 0.3 at% of the decomposition products are N-containing compounds from ethylene diamine decomposition, and less than 2 at% water. XRD patterns of the catalyst at different stages of decomposition only showed silver oxalate and silver (Fig. S5).

The additional minor weight loss around 170 °C in all three gas atmospheres can be attributed to the formation of a passivation layer around the oxalate during the main decomposition step, retarding full decomposition. This behavior of silver oxalate during decomposition was also observed by MacDonald in 1936 and Leiga in 1966 in their research on the decomposition of bulk silver oxalate [63,64]. The ratio of the different weight loss steps depends on the crystal shape and size and hence varies with the preparation method of the silver oxalate and the measurement conditions, as we also confirmed experimentally (Figs. S4–S6) [51].

The results of TGA-MS and XRD show that the decomposition steps are primarily caused by a one-step decomposition of $Ag_2C_2O_4$, drying of the samples before the measurement removed most of the ethylene diamine and water. No major contributions of decomposition of ethylene diamine (*en*) or evaporation of water were observed in the MS results (Fig. S3) and no formation of intermediate products was observed in the XRD during decomposition (Figs. S5 and S6).

The slight shift of weight loss toward lower temperatures during the decomposition in hydrogen is probably caused by its high thermal conductivity rather than by an intrinsically different decomposition mechanism, as is shown in the supplementary information. The decomposition step in at 250 °C in oxidative atmosphere could be caused by the formation of silver oxide during decomposition at lower temperatures, which decomposes around 250 °C. Part of the silver oxalate could have been converted to amorphous Ag_2O, which would not be directly visible in XRD. When all the oxalate would undergo formation of silver oxide and subsequent decomposition to metallic silver a weight loss of 1.05% above 200 °C is expected, while a weight loss of 0.25% is observed. The formation of a small amount of silver oxide most likely explains the larger silver particle sizes obtained in oxidizing atmosphere, as silver oxide is known to be mobile on the support surface [65].

3.4. Temperature dependence of catalytic performance

A typical temperature program and resulting ethylene conversion and selectivity to ethylene oxide are displayed in Fig. 5 for catalyst *$AgAl_2O_3$_100%O2_25*. The spikes at the start of each temperature dwell are caused by an overshoot of the temperature controller, causing similar spikes in conversion and selectivity as is visible in the top left frame. The conversion (orange line) increases steadily with temperature, while the selectivity (blue line) decreases with temperature. In the right frame, the conversion at different temperatures from three catalysts over a range of particle sizes is displayed. The drawn lines represent the fitting with an Arrhenius-type equation. The ethylene conversion levels off at 12%. This is due to the depletion of oxygen from the gas stream (equation S1–S13). Small amounts of CO and acetaldehyde were observed at conversions exceeding 12%. At lower conversions, carbon dioxide and water were the only side products observed. Catalytic key parameters, turnover frequency and selectivity, are calculated from data obtained at conversions below 5%. The absence of external and internal transport limitations at these conditions

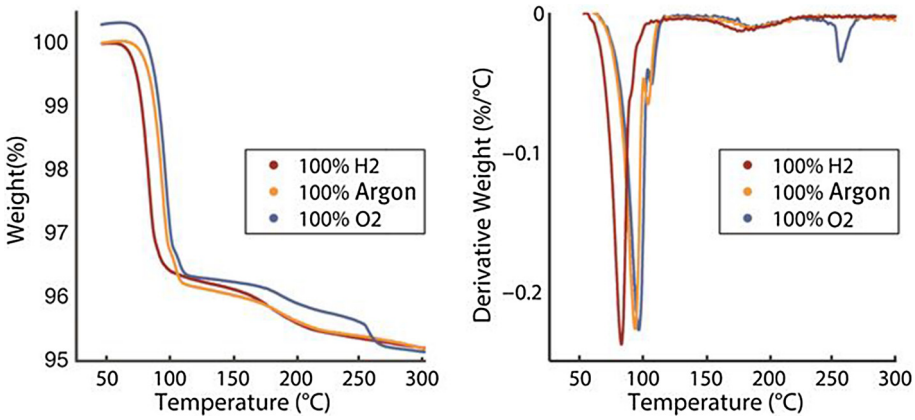

Fig. 4. TGA (left) and DTG (right) of $[Ag(en)_2]_2C_2O_4/\alpha$-$Al_2O_3$ in hydrogen (red), argon (orange) and oxygen (blue) with a flow of 10 mL min^{-1} in a background flow of 20 mL min^{-1} inert. Samples dried in situ in inert gas flow at 70 °C before analysis.

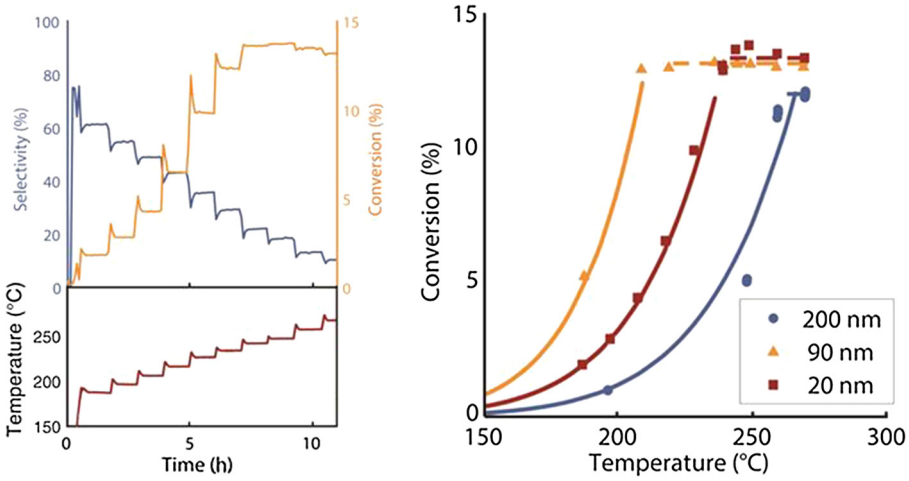

Fig. 5. Conversion of ethylene (orange) and selectivity toward ethylene oxide (blue) of $AgAl_2O_3$_100%O2_25 (top left frame), with corresponding reactor temperature (bottom left frame). Conversion data of three selected catalysts plotted against temperature fitted with an Arrhenius equation (right frame). Data obtained at atmospheric pressure in a temperature range of 180–270 °C with 8.5% O_2 and 30% ethylene flow in helium and a GHSV of 6.000 h^{-1}.

was established by using the Mears and Weisz-Prater criteria (Supplementary information) [66].

The silver time yield (STY) of silver catalysts with different particle sizes, defined as the amount of moles ethylene converted per gram of silver per second, can be found in Fig. 6. The STY of small particles is relatively low and reaches a maximum at a particle size of about 60 nm. Above this size, the STY scales inversely with particle size. The right frame shows the activity per exposed silver surface, better known as the turnover frequency or TOF, which is low for small particles and increases with particle size up to about 60 nm.

The observed decline in STY for larger particles is expected due to a decline in exposed active sites per gram of silver with increasing particle size. The low activity for small particles points to an intrinsic particle size effect. The overall trend in activity is in good agreement with literature where a similar sharp decline in turnover frequency at particle sizes below 60 nm was reported [1,2,25,53]. The observed turnover frequencies agree with those observed in academic as well as patent literature. Details can be found in the supplementary information in section S4 [27,67].

3.5. Particle size dependence of selectivity

The selectivity to ethylene oxide as a function of temperature is displayed in the left frame of Fig. 7 for catalysts with surface averaged particle sizes of 20, 90 and 200 nm. The selectivity decreases linearly with temperature until a certain temperature, after which the decline becomes less pronounced. The steep decline of selectivity with temperature is due to the fact that the selectivity strongly decreases with increasing conversion levels, as will be discussed later. The inflection point in the selectivity corresponds to the temperature at which the conversion flattens off due to oxygen depletion as discussed above. The selectivity of the sample containing 90 nm silver particles decreases with temperature more sharply than the samples containing 20 or 200 nm silver particles. In the right frame in Fig. 7, the selectivity at 190 °C as a function of particle size is shown [25,53]. The particle size dependency at constant temperature corresponds to the trends reported in literature, showing a slight apparent (*vide infra*) increase in selectivity with particle size.

In contrast, the selectivity at a constant conversion of 2.8% plotted in the left frame of Fig. 8 shows no significant particle size

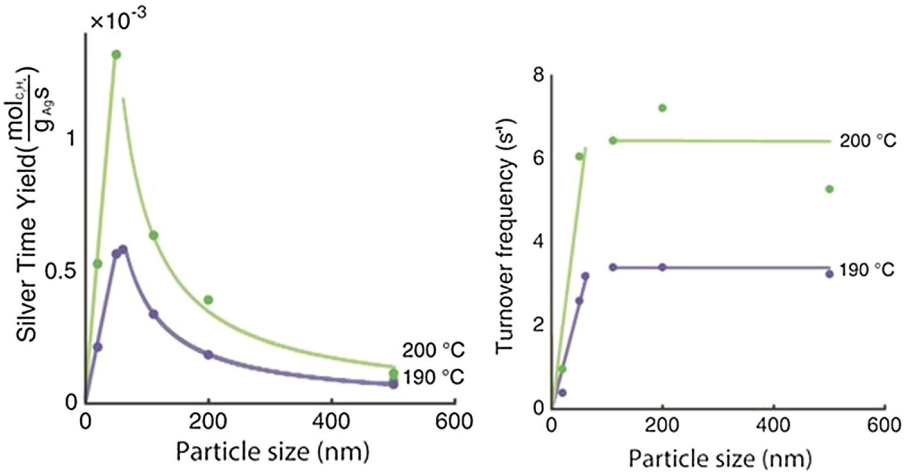

Fig. 6. Silver Time Yield of Ag/α-Al_2O_3 catalysts with different average Ag particle sizes (left frame) and turnover frequency as a function of average Ag particle size for ethylene epoxidation of Ag/α-Al_2O_3 catalysts (right frame). In both frames lines are added to guide the eye. Catalytic data obtained at atmospheric pressure with 8.5% O_2 and 30% ethylene flow in helium and a GHSV of 6.000 h^{-1} at 190 and 200°C and conversions ranging from 0 to 4.5%.

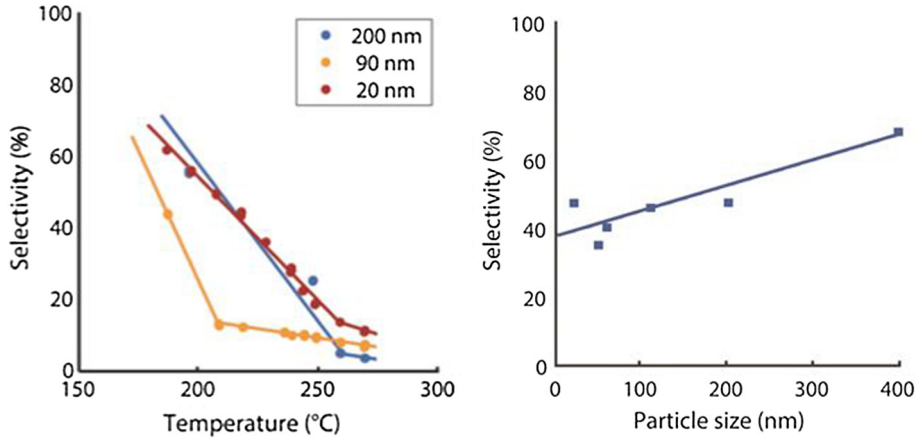

Fig. 7. Selectivity to ethylene oxide as a function of temperature (left) and particle size (right) at 190 °C for ethylene oxidation of Ag/α-Al_2O_3 catalysts. Catalytic data obtained at atmospheric pressure with 8.5% O_2 and 30% ethylene flow in helium and a GHSV of 6.000 h^{-1} with conversions ranging from 0 to 4.5%.

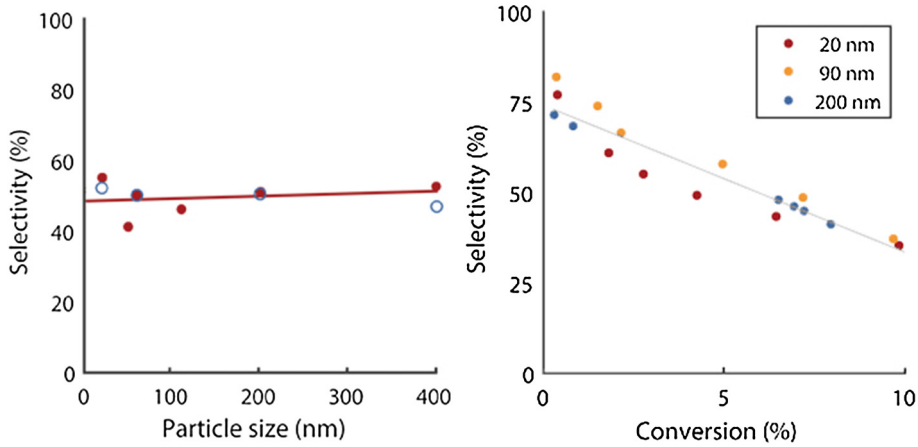

Fig. 8. Selectivity as a function of particle size for ethylene epoxidation of Ag/α-Al_2O_3 catalysts at constant conversion (2.8%, left frame). Selectivity versus conversion of silver catalyzed epoxidation (right). Catalysts with different particle size show that selectivity is conversion dependent, while all three catalysts follow the same trendline.

dependency. In the right frame, the selectivity over the entire conversion range is plotted against the conversion. Different temperatures have been used to obtain the same conversion for catalysts with different particle sizes, the selectivity of all catalysts falls on the same line. It should be noted that this method of varying temperature could introduce differences in selectivity, due to different activation energies of the selective and unselective reaction pathways.

The decrease in selectivity in the left frame of Fig. 7 is caused by an increased rate of the secondary reaction, subsequential oxidation of ethylene oxide. This is due to an increased conversion with temperature, increasing the partial pressure of the primary reactant of this secondary reaction, ethylene oxide. The overall selectivity of the reaction is reduced due to this effect. This also plays a key role in the right frame of this figure. In this frame, the selectivity is reported at constant temperature, but at different conversion. The conversion-dependence of the selectivity introduces a systematic error in the particle size effect.

In the left frame of Fig. 8 the selectivity at constant conversion is reported, both at constant GHSV (open symbols) and at constant temperature (closed symbols). For both cases no apparent particle size dependency can be observed. This shows that the selectivity is primarily conversion-dependent, instead of particle size dependence.

The selectivity data at constant conversion suggest that the selectivity is either particle size independent or only slightly particle size dependent. Points in Fig. 8 have been measured at different temperatures, however calculations (see supplementary information section 4) show that the influence of temperature on selectivity at a given low conversion is very limited. Also the data points that have been obtained at constant temperature (but different flow rates) show that the selectivity is principally particle size independent. While this does not agree with previous results reported in literature, these studies were either performed at constant temperature, which obscures the selectivity with the temperature dependence of conversion, or by using model catalysts consisting of Ag single crystal planes [26,68].

Although we clearly show a strong particle size dependence (for particle sizes below 60 nm) of the intrinsic activity, the selectivity is not significantly affected by particle size in this range. The understanding of this particle size dependence is therefore not straightforward. It might be expected that the occurrency of certain crystal planes, such as the silver (1 0 0) crystal plane, depends on particle size, but there is no consensus in literature that this should have a strong influence on the intrinsic activity for ethylene epoxidation, and one might expect that if this would be an important factor, also the selectivity would be expected to be size dependent [24,26].

Rather it is seems likely that oxygen plays a decisive role. As posed by several authors, the nature of the sites that bind and activate ethylene critically depends on the presence and nature of oxygen on the silver surface [18,20,23,37–39,42,69]. The size dependent activity depicted in Fig. 6 is caused by a very low occurrence of active sites on small silver particles. Generally it has been posed that sites related to "nucleophilic" or "ionic" oxygen are rare for silver particles up to sizes of 30–50 nm [20,37–39,42,70]. However, the fact that we do not observe, in the same particle size region, a dependence of the selectivity on particle size, implies that the concentration of these active ethylene binding sites does not determine the selectivity of the reaction. In other words, it determines the activation of the ethylene molecule, but not its fate, while apparently there are no alternative binding sites on the silver that lead to conversion. Dedicated measurements on the dependence of the occurrency of the different oxygen containing sites as a function of Ag particle size and correlating them to activity and selectivity observed could shed further light on this phenomenon.

4. Conclusion

A study of the synthesis of supported silver catalysts by decomposition of silver oxalate showed that different silver particle sizes can be obtained without changing the weight loading or the catalyst precursor, by using different gas atmospheres. The obtained particle sizes were in a range of 20–500 nm, with hydrogen gas treatment yielding 20 nm silver particles. While the catalysts have different average silver particle sizes, the support and metal loading are identical. The clear surface plasmon resonance absorption by small silver particles observed in UV/Vis correlates with particle sizes from electron microscopy techniques (SEM and TEM) and can therefore be used as a fast and statistically relevant analysis technique for the silver particle size.

The effect of the particle size on the ethylene epoxidation *activity* is in good agreement with literature. This shows the validity of our synthesis method. We additionally show that the *selectivity* is strongly dependent on conversion. This means that reporting the selectivity at a constant temperature, as is commonly done in relevant literature, introduces major artifacts. When the selectivity is reported at constant conversion, no clear particle size dependence of selectivity was observed, in contrast to most literature reports. While different silver crystal planes may have different selectivities to ethylene oxide as indicated by surface science experiments [23,24,26], the particle size independence of the selectivity shows that this does not play an important role in more industrially relevant model catalysts, like the ones studied here.

Acknowledgements

This research was funded by NWO Vici project no. 16.130.344.

The authors would like to thank Jan-Willem de Rijk for the DSC measurements, Carlo Buijs and Marlies Coolen-Kuppens for their help on the epoxidation setup, Helen de Waard (Geochemistry, Utrecht University) for the ICP analysis. We would like to acknowledge Lisette Pompe for the TEM measurements and support from the European Research Council, EU FP7 ERC Advanced Grant no. 338846 for funding of the TEM measurement time.

Appendix A. Supplementary material

Supplementary data associated with this article can be found, in the online version, at https://doi.org/10.1016/j.jcat.2017.10.001.

References

[1] S. Rebsdat, D. Mayer, Ullmann's Encycl. Ind. Chem. (2012) 547–572.
[2] H. Kestenbaum, A. Lange de Oliveira, W. Schmidt, F. Schüth, W. Ehrfeld, K. Gebauer, H. Löwe, T. Richter, D. Lebiedz, I. Untiedt, H. Züchner, Ind. Eng. Chem. Res. 41 (4) (2002) 710–719.
[3] G.C.C. Mendes, T.R.S. Brandão, C.L.M. Silva, Am. J. Infect. Control 35 (9) (2007) 574–581.
[4] M. Lazaridis, H.A. Little, C.B. Meyer, K.K. Pathiyal, 1(12) (2001).
[5] M. Argyle, C. Bartholomew, Catalysts 5 (1) (2015) 145–269.
[6] Z. Łodziana, J.K. Nørskov, P. Stoltze, J. Chem. Phys. 118 (24) (2003) 11179.
[7] S. Rojluechai, S. Chavadej, J.W. Schwank, V. Meeyoo, Catal. Commun. 8 (1) (2007) 57–64.
[8] C. Petitto, G. Delahay, Catal, Letters 142 (4) (2012) 433–438.
[9] P. Raharjo, C. Ishizaki, K.J. Ishizaki, Ceram, Soc. Japan 108 (1257) (2000) 449–455.
[10] J.K. Lee, X.E. Verykios, R. Pitchai, Appl. Catal. 44(C) (1988) 223–237.
[11] C.-F. Mao, M. Albert Vannice, Appl. Catal. A Gen. 122 (1) (1995) 61–76.
[12] A.M. Lauritzen, Ethylene Oxide Catayst and Process for Preparing the Catalyst, 1988.
[13] M.O. Özbek, R.A. van Santen, Catal, Letters 143 (2) (2013) 131–141.
[14] P.A. Kilty, W.M.H. Sachtler, Catal. Rev. Sci. Eng. 1974 (10) (2012) 1–16.
[15] E.A. Carter, W.A. Goddard, J. Catal. 112 (1) (1988) 80–92.
[16] C.T. Campbell, M.T. Paffett, Surf. Sci. 139 (2–3) (1984) 396–416.
[17] C.T. Campbell, J. Vac. Sci. Technol. A Vac. Surf. Film 2(2) (1984) 1024–1027.
[18] R.A. Van Santen, H.P.C.E. Kuipers, Advances in Catalysis, vol. 23, 1987, pp. 265–321.
[19] A. Ayame, T. Kimura, M. Yamaguchi, H. Miura, N. Takeno, H. Kanoh, I. Toyoshima, J. Catal. 100 (2) (1986) 401–413.
[20] R.B. Grant, R.M. Lambert, J. Catal. 92 (2) (1985) 364–375.
[21] S. Linic, M.A. Barteau, J. Am. Chem. Soc. 124 (2) (2002) 310–317.
[22] S. Linic, M.A. Barteau, J. Catal. 214 (2) (2003) 200–212.
[23] M.O. Özbek, I. Önal, R.A. van Santen, ChemCatChem 3 (1) (2011) 150–153.
[24] P. Christopher, S. Linic, ChemCatChem 2 (1) (2010) 78–83.
[25] X. Verykios, F.P. Stein, R.W. Coughlin, J. Catal. 66 (1980) 368–382.
[26] P. Christopher, S. Linic, J. Am. Chem. Soc. 130 (34) (2008) 11264–11265.
[27] C.T. Campbell, J. Catal. 444 (1985) 436–444.
[28] J.C. Wu, P. Harriott, J. Catal. 39 (3) (1975) 395–402.
[29] G.L. Bezemer, J.H. Bitter, H.P.C.E. Kuipers, H. Oosterbeek, J.E. Holewijn, X. Xu, F. Kapteijn, A.J. van Dillen, K.P. de Jong, J. Am. Chem. Soc. 128 (12) (2006) 3956–3964.
[30] R. Van Den Berg, G. Prieto, G. Korpershoek, L.I. Van Der Wal, A.J. Van Bunningen, S. Lægsgaard-jørgensen, P.E.De Jongh, K.P. De Jong, 2016.
[31] R. Van Hardeveld, F. Hartog, Surf. Sci. 15 (2) (1969) 189–230.
[32] P. Van Helden, I.M. Ciobîc, R.L.J. Coetzer, 261 (2016), 48–59.
[33] X.E. Verykios, F.P. Stein, R.W. Coughlin, Catal. Rev. 22 (2) (1980) 197–234.
[34] D.J. Sajkowski, M. Boudart, Structure Sensitivity of the Catalytic Oxidation of Ethene by Silver, vol. 29, 1987.
[35] J.K. Lee, X.E. Verykios, R. Pitchai, Appl. Catal. 50 (1) (1989) 171–188.
[36] S.N. Goncharova, E.A. Paukshtis, B.S. Bal'zhinimaev, Appl. Catal. A Gen. 126 (1) (1995) 67–84.
[37] V.I. Bukhtiyarov, I.P. Prosvirin, R.I. Kvon, S.N. Goncharova, B.S. Bal'zhinimaev, J. Chem. Soc. Faraday Trans. 93 (13) (1997) 2323–2329.
[38] V.I. Bukhtiyarov, A.F. Carley, L.A. Dollard, M.W. Roberts, Surf. Sci. 381 (1997) L605–L608.
[39] V.I. Bukhtiyarov, V.V. Kaichev, J. Mol. Catal. A Chem. 158(1) (2000) 167–172.
[40] V.M. Mastikhin, S.N. Goncharova, V.M. Tapilin, V.V. Terskikh, B.S. Balzhinimaev, J. Mol. Catal. A Chem. 96(2) (1995) 175–179.
[41] L.M. Akella, H.H. Lee, J. Catal. 86 (2) (1984) 465–472.
[42] V.I. Bukhtiyarov, M. Havecker, V.V. Kaichev, A. Knop-Gericke, R.W. Mayer, R. Schlogl, Phys. Rev. B 67 (23) (2003) 235422.
[43] S.-G. Kim, Y.-G. Seo, Y.-J. Cho, J.-S. Shin, S.-C. Gil, W.-M. Lee, Bull. Korean Chem. Soc. 31 (7) (2010) 1891–1896.
[44] P.J. Van den Hoek, E.J. Baerends, R.A. Van Santen, J. Phys. Chem. 93 (17) (1989) 6469–6475.
[45] M. Casavola, J. Hermannsdörfer, N. de Jonge, A.I. Dugulan, K.P. de Jong, Adv. Funct. Mater. 25 (33) (2015) 5309–5319.
[46] J.P. den Breejen, P.B. Radstake, G.L. Bezemer, J.H. Bitter, V. Frøseth, A. Holmen, K.P. de Jong, J. Am. Chem. Soc. 131 (20) (2009) 7197–7203.
[47] T. Toupance, M. Kermarec, C. Louis, (2000) 965–972.
[48] J.R.A. Sietsma, J.D. Meeldijk, J.P. Den Breejen, M. Versluijs-helder, A.J. Van Dillen, P.E. De Jongh, K.P. De Jong 3(3) (2007) 4631–4633.
[49] P. Munnik, M. Wolters, A. Gabrielsson, S.D. Pollington, G. Headdock, J.H. Bitter, P.E. De Jongh, K.P. De Jong, J. Phys. Chem. C 115(30) (2011) 14698–14706.
[50] S.M. Pourmortazavi, S.S. Hajimirsadeghi, I. Kohsari, R. Fareghi Alamdari, M. Rahimi-Nasrabadi, Chem. Eng. Technol. 31 (10) (2008) 1532–1535.
[51] V.V. Boldyrev, Thermochim. Acta 388 (1–2) (2002) 63–90.
[52] A.R. Fiorucci, L.M. Saran, É.T.G. Cavalheiro, E.A. Neves, Thermochim. Acta 356 (1–2) (2000) 71–78.
[53] J. Jiang, T. Xu, Y. Li, X. Lei, H. Zhang, D.G. Evans, X. Sun, X. Duan, Bull. Korean Chem. Soc. 35 (6) (2014) 1832–1836.
[54] R.P. Nielsen, J.H. La Rochelle, Patent catalyst for production of ethylene oxide, 1976.
[55] E. Plessers, I. Stassen, S.P. Sree, K.P.F. Janssen, H. Yuan, J. Martens, J. Hofkens, D. De Vos, M.B.J. Roeffaers, ACS Catal. 5 (11) (2015) 6690–6695.

[56] J. Hoekstra, A.M. Beale, F. Soulimani, M. Versluijs-Helder, J.W. Geus, L.W. Jenneskens, New J. Chem. 39 (8) (2015) 6593–6601.
[57] J.J. Mock, M. Barbic, D.R. Smith, D.A. Schultz, S. Schultz, J. Chem. Phys. 116 (15) (2002) 6755–6759.
[58] T.A. Nijhuis, Towards a new propene epoxidation process, 1997.
[59] P. Harriott, J. Catal. 21 (1) (1971) 56–65.
[60] A.G.M. da Silva, T.S. Rodrigues, J. Wang, L.K. Yamada, T.V. Alves, F.R. Ornellas, R. A. Ando, P.H.C. Camargo, Langmuir 31 (37) (2015) 10272–10278.
[61] V. Amendola, O.M. Bakr, F. Stellacci, Plasmonics 5 (1) (2010) 85–97.
[62] A. Liebsch, Phys. Rev. B 48 (15) (1993) 11317–11328.
[63] A.G. Leiga, J. Phys. Chem. 70 (10) (1966) 3254–3259.
[64] J.Y. Macdonald, Nature 137 (3456) (1936) 152–153.
[65] N.M. Wichner, J. Beckers, G. Rothenberg, H. Koller, J. Mater. Chem. 20 (19) (2010) 3840–3847.
[66] H.S. Fogler, in: N.R. Amundson (ed.), Elements of Chemical Reaction Engineering, third ed., Prentice Hall International, 1999.
[67] W.E. Evans, P.I. Chipman, United States Patent. US 6717011 B2, 2004.
[68] R.A. Van Santen, Acc. Chem. Res. 42 (1) (2009) 57–66.
[69] A.M. Sorokin, I.P. Prosvirin, D.V. Demidov, V.I. Bukhtiyarov 2(2) (2013) 1–4.
[70] R.B. Grant, R.M. Lambert, Surf. Sci. 146 (1) (1984) 256–268.